COBEM UBERLÂNDIA 2019

ABCM Associação Brasileira de Engenharia e Ciências Mecânicas

25th ABCM International Congress of Mechanical Engineering
October 20-25, 2019, Uberlândia, MG, Brazil

NUMERICAL INVESTIGATION OF AN ISOTHERMAL SWIRLING FLOW

Everton de Souza Ribeiro[1]
Ricardo de Vasconcelos Salvo[2]
Rodrigo Corrêa da Silva[3]
Rafael Sene de Lima[4]
Ismael de Marchi Neto[5]
Federal University of Technology - Parana, Estrada dos Pioneiros, 3131, Londrina, Brazil
[1]evertonribeiro@alunos.utfpr.edu.br, [2]ricardosalvo@utfpr.edu.br, [3]rodrigosilva@utfpr.edu.br, [4]rafaellima@utfpr.edu.br, [5]ismaelneto@utfpr.edu.br

Abstract. *Numerical simulations of an isothermal swirling flow generated by a burner was carried employing OpenFOAM. The geometry, operating conditions and velocity measurements of the combustion chamber were reported in literature. The numerical results were obtained by applying Large Eddy Simulation (LES) -Smagorinsk approach and compared with experimental results obtained employing the volumetric three-components velocimetry (V3V) technique. 3D-geometry consisted of hexahedral mesh and included the swirler located within the burner. Large scale structures were identified applying Q-criterion as well as pressure and velocity isosurfaces. Comparisons of numerical and experimental data indicated LES approach was able to predict the flow envelope and peak velocities. A large and central inner recirculation zone in the vicinity of burner was generated due to both swirling effect and burner geometry. In opposite to the experimental data, numerical results showed a symmetrical flow, possibly as a result of either boundary conditions or geometry simplification. Nevertheless, radial profiles of axial and tangential velocities indicated large gradients were reasonably well captured by the simulations. Other parameters such as width of internal recirculation zone, minimum axial velocity and mass flow recirculation indicated simulations reproduced the flow with satisfactory accuracy.*

Keywords: *Swirling flow, Large Eddy Simulation (LES), OpenFOAM, Large scale structures*

1. INTRODUCTION

The Paris Agreement established several milestones in order to reduce greenhouse gas emissions, encouraging R&D activities in the field of energy efficiency and new energy sources (UNFCCC, 2015). In this context, Brazil has committed to reduce 43% of its greenhouse gas emission from 2005 level until 2030 (MMA, 2015). According to Corrêa da Silva *et al.* (2016) renewable energy sources such as wind, solar, and biomass will play an important role to fulfill this goal. The replacement of traditional fuels by renewable energy is also a strategy to reduce pollutant emissions and oil dependency. Biogas and biomethane are pointed out as promising options for natural gas (NG). Both renewable sources have been growing worldwide due its lower costs and environmentally friendly aspects in comparison to traditional fossil fuels (HOLEWA *et al.*, 2013). Colorado *et al.* (2010) reported experimental investigation comparing biogas and NG combustion, attesting the compatibility of the biogas with the current combustion systems, requiring only minor modifications. It also stated similar furnace efficiency and combustion characteristics, as temperature and pollutants formation, in biogas combustion compared with NG. According to Corrêa da Silva *et al.* (2016) is expected that biomass energy contribution, including biogas, in the Brazilian energy mix increase by 41.7% until 2023 in comparison with 2013.

A major limitation of employing low quality gaseous fuels is flame stabilization. A widely spread technique to enhance mixture between oxidant and fuel and provide flame stabilization in burners are swirling flows. Emissions could also be reduced employing swirling flames, as previously demonstrated by Corrêa da Silva and Krautz (2014) a correlation between swirl intensity and emissions. Computational fluid dynamics (CFD) simulations have been successfully applied to predict flow behavior in combustion engineering applications such as burners and furnaces. Combustion chemistry reactions and heat transfer models could also be coupled to improve the analysis (Baukal, 2003). The simulation results allow the study of aerodynamics and fuel-oxidant mixing characteristics, which are key parameters in flame structure, stability, and pollutant emissions. Cost reduction, improvements in efficiency, safety, and lifetime extension are some benefits of employing this technique. In addition, certain burner conditions might be impractical to evaluate experimentally due safety restrictions and CFD becomes a viable option. However, simulation of swirling flow might be challenging because of large velocity gradients and reliable predictions depend on the accuracy of turbulence models. Most of used turbulence models are based on the Reynolds Averaged Navier-Stokes (RANS) equations and the Large Eddy Simulation

(LES) methodology. The RANS approach is widely spread due its satisfactory results and for requiring less computational effort than LES-based models. Nevertheless, the LES allows simulating complex unsteady turbulent flows, improving accuracy and quality of results according to Vashahi and Lee (2018). LES predictions can be further explored by analyzing turbulent oscillations with help of investigation of large-scale structures, essential for understanding turbulent mixing, energy and mass transport, as well as flow stability.

In this paper a Large Eddy Simulation (LES) of an isothermal swirling flow generated by a gas burner is fully presented. The numerical results were compared against a novel technique called volumetric three-components velocimetry (V3V) (Boushaki *et al.*, 2017a).

2. METHODOLOGY

2.1 LES governing equations

Mass and momentum conservation equations applied to isothermal and incompressible flow adopting the Einstein convention (H. Ferziger and Peric, 2002) are presented in Eq. (1) and Eq. (2). For turbulence modeling is employed the Large Eddy Simulation (LES). In this approach, a filtering process separates the motion large scales from the smallest ones. Smallest scales are not solved in LES and therefore must be modeled. In this work, the Smagorinsky model is employed as described in Smagorinsky (1963).

$$\frac{\partial \rho \bar{u_i}}{\partial x_i} = 0, \tag{1}$$

$$\frac{\partial \rho \bar{u_i}}{\partial t} + \frac{\partial}{\partial x_j}(\rho \bar{u_i} \bar{u_j}) = \frac{\partial \bar{p^*}}{\partial x_i} + \frac{\partial}{\partial x_j}\left[\mu + \mu_t \left(\frac{\partial \bar{u_i}}{\partial x_j} + \frac{\partial \bar{u_j}}{\partial x_i}\right)\right], \tag{2}$$

$$\bar{p^*} = \bar{p} + \frac{2}{3}\rho k, \tag{3}$$

In Eq. (1) and Eq. (2), the overbar denotes a filtered quantity. In Eq. (1), the asterisk denotes the modified pressure Eq. (3), κ was the subgrid turbulence kinetic energy and μ_t is the turbulent viscosity, which represents the energy dissipation in the smallest flow scales.

$$\mu_t = \rho (C_s \Delta)^2 \left|\bar{S}\right|, \tag{4}$$

Δ is the grid filter length and $\left|\bar{S}\right|$ is the filtered shear strain rate (5) and C_s is the Smagorinsk Coefficient given by Eq. (6) presented by Sullivan *et al.* (1994):

$$\left|\bar{S}\right| = \sqrt{\bar{S_{ij}} \bar{S_{ij}}}, \text{ and } \bar{S_{ij}} = \frac{1}{2}\left(\frac{\partial \bar{u_i}}{\partial x_j} + \frac{\partial \bar{u_j}}{\partial x_i}\right), \tag{5}$$

$$C_s = \left(C_k \sqrt{\frac{C_k}{C_\epsilon}}\right)^{\frac{1}{2}}, \tag{6}$$

C_k and C_ϵ are constants, taken here respectively as 1.05 and 0.07. The total viscosity is given by the sum of the turbulent and molecular viscosities. Here, the term C_s is a parameter to be determined and it varies according to the type of flow, the Reynolds number, the grid resolution, and several other parameters. Another difficulty associated with the utilization of this model is that the turbulent viscosity does not reduce itself near to the wall. A common practice to overcome this limitation is the use of Van Driest wall damping function H. Ferziger and Peric (2002). In OpenFOAM the damping function is derived from filter width, changing it according to the wall distance Eq. (7) according to (Penttinen *et al.*, 2011):

$$\Delta = min\left(\Delta_{mesh}, \left(\frac{k}{C_\Delta}\right)\right) y \left(1 - e^{-y^+/A^+}\right), \tag{7}$$

Δ_{mesh} is the cubic root of the cell volume, k is the von Kámán constant, y^+ and y describes the distance to wall surface (the first one is dimensionless), C_Δ and A^+ are constants, equal to 0.158 and 26, respectively.

2.2 Numerical setup

The OpenFOAM software is used to solve the set of governing equations. A steady-state initial solution is obtained by using a κ-epsilon RANS turbulence model and applied as initial velocity field in LES. A Semi-Implicit Method for Pressure Linked Equations (SIMPLE) is applied as pressure-velocity coupling scheme for this initial step. LES-Smagorinsk

turbulence model and Pressure Implicit with Split Operator (PISO) velocity-pressure coupling are applied in the simulation. A second order backward scheme is used for timing advancement while central difference scheme (Gauss Linear) is applied for spatial discretization. The average numerical results are obtained applying a 10 seconds time sample.

A Beowulf cluster with ten nodes is applied throughout this study. Each node has an Intel i7 6700K, 8 GB of DDR3-1600 MHz of RAM, and 1 TB of HD. A one gigabit ethernet network is available to connect the cluster.

2.3 Meshes

All meshes represent the full 3D geometry, including the swirler located within the burner. The only difference between experimental and numerical geometries is the holes located in the central pipe. The eight holes for injecting the fuel are simplified to a single surface with same area (see Section 2.6 for more details on burner geometry). Hexahedral elements are applied due to their smaller diffusion. A mesh with 4.15 million cells was able to produce satisfactory results. Time-step dependency was checked in previous study, and a time-step of 1E-5 seconds is also applied.

2.4 Q-criterion

Large scales structures are commonly related in literature as vortex structures. Hunt *et al.* (1988) presented the first vortex criterion (Q), i.e. Q-criterion, for a three-dimensional vortex, written in terms of the vorticity tensor (ω_{ij}) and are rate-of-strain tensor (D_{ij}). This equation defines vortex as a spatial region where the rotational tensor overcomes the rate-of-strain, according to Haller (2005).

$$\omega_{ij} = \frac{1}{2}\left[\frac{\partial u_i}{\partial x_j} - \frac{\partial u_j}{\partial x_i}\right], \tag{8}$$

$$\mathrm{D}_{ij} = \frac{1}{2}\left[\frac{\partial u_i}{\partial x_j} + \frac{\partial u_j}{\partial x_i}\right], \tag{9}$$

$$\mathrm{Q} = \frac{1}{2}\left[|\omega_{ij}|^2 - |\mathrm{D}_{ij}|^2\right] > 0, \tag{10}$$

2.5 IRZ characterization

The IRZ is defined as the region with negative axial velocity, indicating a reverse flow region, as defined by Leibovich (1978), characterized by as a low-pressure region. Some parameters were defined in order to compare the IRZ captured by the numerical methods and the experimental results. The IRZ width (Eq. (11)) was defined as the difference between the furthest west (PW)and east (PE) positions where the axial velocity present negative values. The minimum axial velocity was defined as the minimum axial velocity at given axial position y/Db (Eq (12)). The mean negative axial velocity was defined by the Eq (13) and Eq. (14) defines the ration between the mass recirculating by the IRZ ($\dot{m}_{rec}$) and the total mass input in the system ($\dot{m} = \dot{m}_{oxi} + \dot{m}_{fuel}$).

$$L_{IRZ} = PW - PE, \tag{11}$$

$$v_{min} = min(v(x, y/Db, 0)), \tag{12}$$

$$\bar{v} = \frac{1}{L_{IRZ}}\int_{PW}^{PE} v\mathrm{dx}, \tag{13}$$

$$\frac{\dot{m}_{rec}}{\dot{m}_{total}} = \frac{\rho\pi L_{IRZ}\int_{PW}^{PE} v\mathrm{dx}}{\dot{m}_{oxi} + \dot{m}_{fuel}}. \tag{14}$$

2.6 Geometry description and boundary conditions

Numerical simulations are performed according to experiments carried out at the *Institut de Combustion Aérothermique Réactivité et Environnement* by Boushaki *et al.* (2017b,a); Merlo *et al.* (2014, 2013). The burner is arranged by two coaxial cylinders (outer and inner diameters of 38 mm and 15 mm) and it is attached at the bottom of the combustion chamber. The burner combines a bluff-body and swirling flow strategy for stabilizing the flame. The swirler is placed within in the annular part at 60 mm upstream the burner exit. In this numerical study only the 1.4 swirl number is investigated. A total of eight holes (diameter of 3 mm) are radially distributed very close to burner's exit plane to inject the fuel. During isothermal experimental studies air is supplied to replace the fuel. The combustion chamber has a square cross-section of 480 mm and height of 1000 mm and operates at atmospheric pressure. Velocity data are obtained with volumetric three-component velocimetry (V3V). Further information on the burner geometry and operating conditions

Table 1: Burner operating conditions (Boushaki *et al.* (2017b)).

Specie	Mass flow rate (kg/h)	Reynolds number
Oxidant	18.504	7000
Fuel	1.080	1490 to 2100

can be found in Mansouri and Boushaki (2018), Boushaki *et al.* (2017a), Boushaki *et al.* (2017b), Merlo *et al.* (2014) and Merlo *et al.* (2013). An overview of combustion chamber and burner are shown in Fig. 1 and the operating conditions are summarized in Tab. 1.

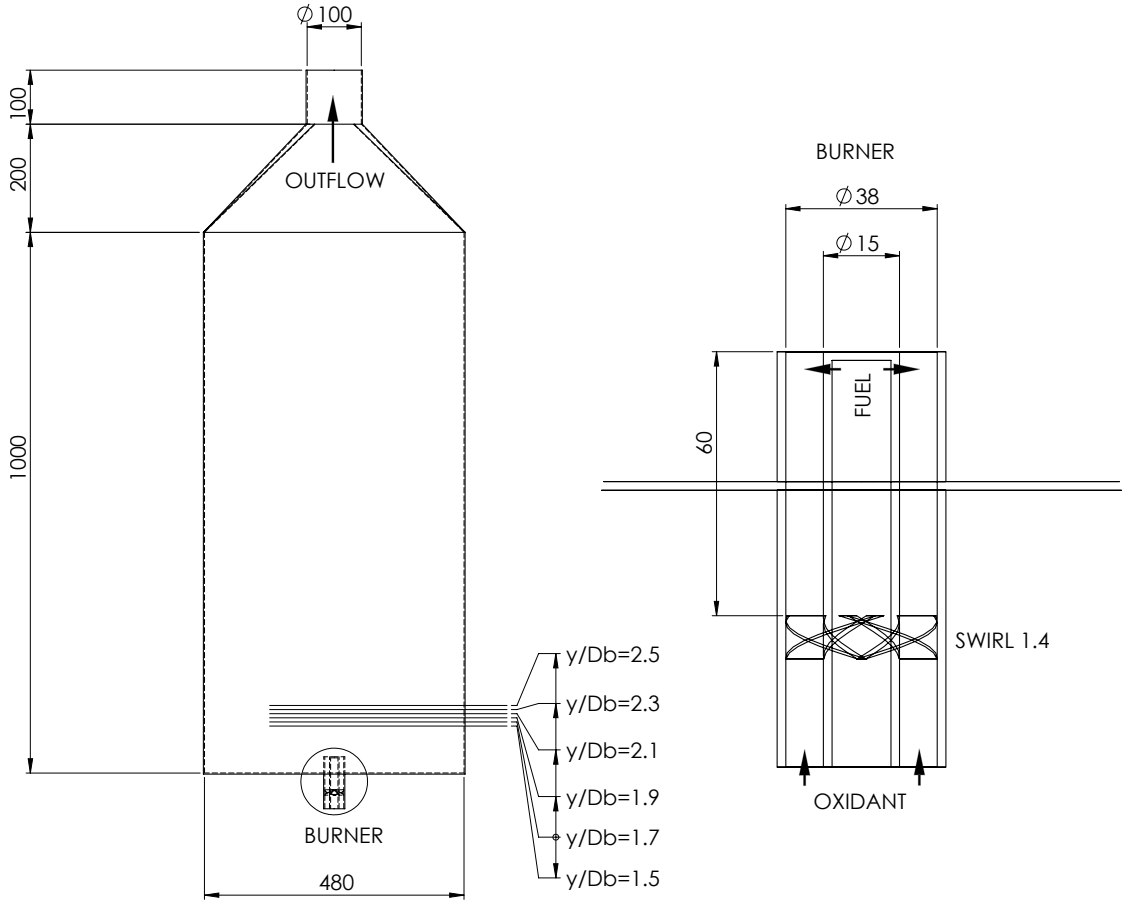

Figure 1: Schematics of combustion chamber and burner geometry (units in mm).

3. RESULTS

3.1 Axial and tangential velocity profiles

Axial mean velocity profiles at six axial positions (Fig. 1) are shown in Fig. 2. The numerical results are compared with experimental data obtained by V3V technique. A strong IRZ is generated in the vicinity of the burner, characterized by a negative axial velocity. Around the IRZ it is possible to identify a high velocity zone (HVZ), a region with large velocity gradient and shear layers. Also, it is possible to identify a radial expansion of the HVZ as the flow moves downstream. This radial expansion of the HVZ is followed by decrease in negative axial velocity, related to the IRZ. In the tangential velocity profiles it is possible to identify a clockwise swirling rotation, and the radial expansion of the HVZ. This radial expansion is explained by the VB phenomena, with the presence of an internal stagnation point that deflects the flow around an aerodynamic blockage.

Both numerical and experimental data show a similar flow behavior. Velocity field predicted by numerical simulations is symmetrical. On the other hand, experimental data indicate the flow is slightly shifted to one side. Previous papers of the ICARE Boushaki *et al.* (2017b); Merlo *et al.* (2014) also identified a symmetrical flow field in reacting and non-reacting conditions, employing the Stereo Particle Image Velocimetry (S-PIV) measurement technique. As explained previously, the VB phenomena could be not only asymmetrical, but also highly time dependent (Lucca-Negro and O'Doherty, 2001).

y/Db	Mass recirculation	Min. velocity	Width IRZ	Negative mean velocity
1.5	14.0%	7.7%	14.1%	1.9%
1.7	41.2%	18.7%	33.4%	21.6%
- 1.9	44.7%	23.3%	35.3%	25.1%
2.1	42.5%	16.1%	37.3%	21.1%
2.3	29.1%	20.2%	20.6%	14.5%
2.5	29.2%	22.1%	18.9%	15.7%

Additionally, previous experience of authors pointed out that some experimental conditions of the flow upstream of the burner could produce asymmetries in the flow pattern downstream. Better predictions for axial velocity profiles where achieved in regions with y/Db higher than 2.1, with similar minimum and maximum velocities. This is also true for the tangential velocity profiles, with experimental and numerical profiles overlapping in several radial locations.

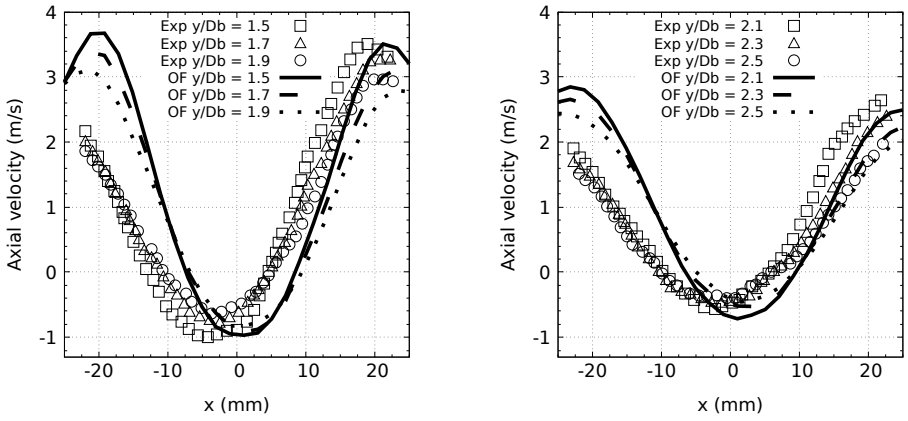

(a) (b)

Figure 2: Axial velocity profiles at several axial distances.

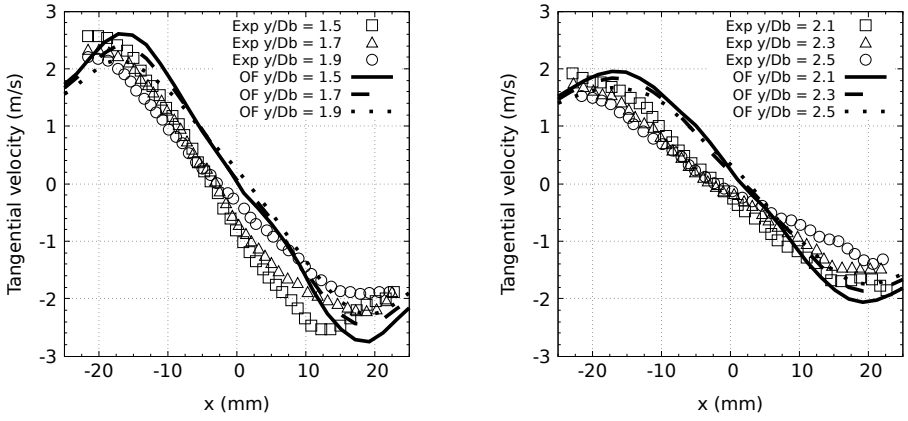

(a) (b)

Figure 3: Tangential velocity profiles at several axial distances.

Table 2 shows percentage differences between the numerical and experimental approaches employing comparative parameters of the IRZ such as width, minimum axial velocity, and normalized mass flow recirculation, calculated using the Eqs. 11, 12, 13 and 14 . The width of the IRZ was reasonable well calculated by numerical approach with a maximum difference of 37.3% against the experimental data. In addition, the maximum negative velocity indicated discrepancies around 23.3%. Normalized mass flow recirculation pointed out a maximum difference of 44.7% between numerical and experimental data. It is important to note that numerical and experimental results have the same order of magnitude, and this discrepancies are mostly due to the asymmetric experimental behavior.

3.2 Large scale structures

Figure 4 shows presents large scale structures in the flow field, (a) employing positive gauge pressure iso-surfaces and (b) Q-criterion methodology. In the positive gauge pressure iso-surfaces is clearly identified helical structures near the burner exit plane, a common type of large scale structure in swirling flows. Downstream the helical structures are rapidly dissipated into smaller structures with random distribution. Others minor structures, including small vortex structures and pressure fluctuations are also shown. The IRZ envelope, defined as a negative gauge pressure zone, are not shown in the present figure. The second figure presents connected fluid regions with positive second invariant of the velocity gradient tensor, as defined by the Eq. 10, highlighting others large scale structures. In this analysis are possible to identify spiral like structures, finger structures and some others minor fluctuations. As explained previously, a HVZ occurs near the burner exit plane, a region with large velocity gradients and shear layers. This characteristics indicated that the spiral like structures observed are caused by the Kelvin–Helmholtz instability, presenting structures orthogonal to the streamwise direction of the flow. Downstream the Kelvin-Helmholtz instabilities become unstable appears as finger like structures. This structures arise as the spiral like structures are almost dissipated. Further downstream almost all the large structures are completely dissipated, remaining only some minor fluctuations.

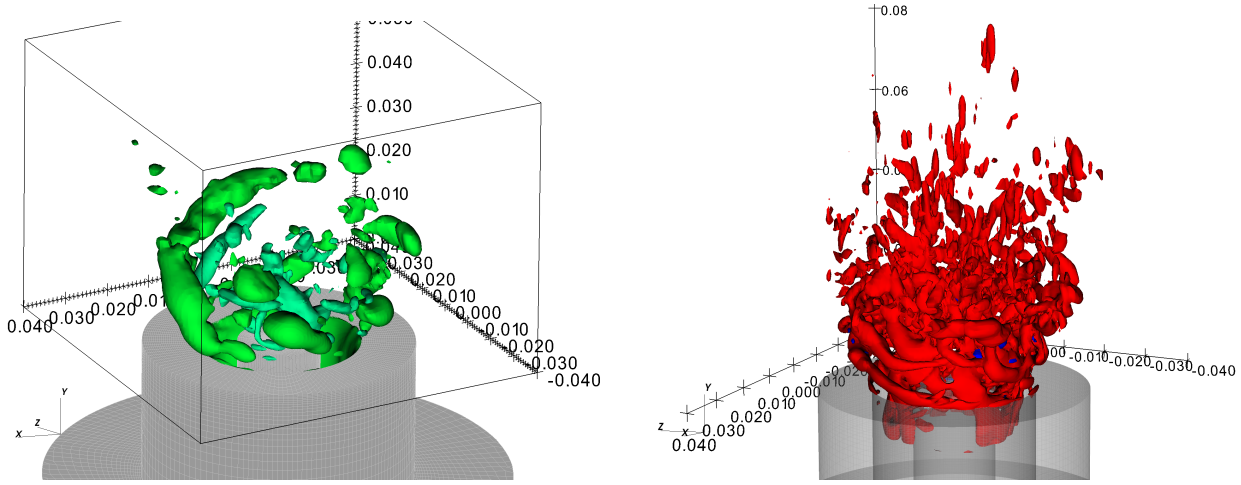

(a) Positive gauge pressure iso-surfaces (b) Q-criterion

Figure 4: Large scales structures.

Figure 5 shows the IRZ in the burner vicinity calculated by the numerical simulation (a) and experiments (b). Selected streamlines revealed the flow path around the IRZ. Colormap slices indicated the magnitude of axial velocity and velocity vectors field. Both approaches shared similar characteristics, such as width, height, and velocity field of the IRZ, showing a good agreement in the volume portion monitored by the V3V. At the IRZ surroundings is possible to identify the HVZ clearly and the radial expansion, as previously observed at the velocity profiles. Large velocity gradient region promotes shear layers and vorticity, leading to vortex formation.

4. CONCLUSION

An isothermal swirling flow generated by a burner is numerically investigated with help of OpenFOAM. LES-Smagorinsk is employed as turbulence modeling. Numerical results are compared with experimental data obtained with a V3V technique. A hexahedral mesh of 4.15 million elements is applied in combination with a time-step advancement of 1E-05 seconds. Overall, this numerical approach is able to predict the flow field in the vicinity of burner. Vortex breakdown is identified and carefully evaluated in this study. Although both approaches presented similar flow behavior, a slightly shifted axial velocity does not occur as indicated by the experimental data. Deviations between numerical and experimental data are less than 45% for IRZ characterization. Also was performed an analysis of large scale structures, identifying the major structures present flow field.

5. ACKNOWLEDGEMENTS

The authors acknowledge the Araucaria Foundation and Federal University of Technology Parana (UTFPR).

6. REFERENCES

Baukal, C., 2003. *Industrial Burners Handbook*. Industrial Combustion. CRC Press. ISBN 978-0-203-48880-5.

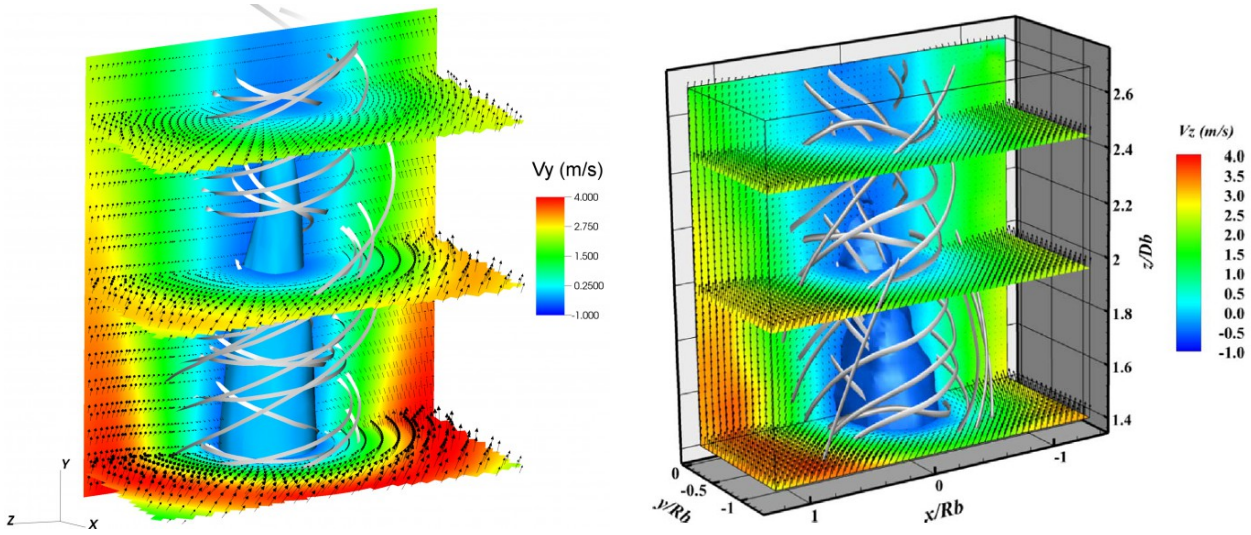

(a) LES (b) V3V

Figure 5: Internal recirculation zone and streamlines.

Boushaki, T., Koched, A., Mansouri, Z. and Lespinasse, F., 2017a. "Volumetric velocity measurements (v3v) on turbulent swirling flows". *Flow Measurement and Instrumentation*, Vol. 54, pp. 46–55. ISSN 0955-5986. doi: 10.1016/j.flowmeasinst.2016.12.003.

Boushaki, T., Merlo, N., Chauveau, C. and Gökalp, I., 2017b. "Study of pollutant emissions and dynamics of non-premixed turbulent oxygen enriched flames from a swirl burner". Vol. 36, No. 3, pp. 3959–3968. ISSN 1540-7489. doi:10.1016/j.proci.2016.06.046.

Colorado, A.F., Herrera, B.A. and Amell, A.A., 2010. "Performance of a flameless combustion furnace using biogas and natural gas". Vol. 101, No. 7, pp. 2443–2449. ISSN 0960-8524. doi:10.1016/j.biortech.2009.11.003.

Corrêa da Silva, R., de Marchi Neto, I. and Silva Seifert, S., 2016. "Electricity supply security and the future role of renewable energy sources in brazil". Vol. 59, pp. 328–341. ISSN 1364-0321. doi:10.1016/j.rser.2016.01.001.

Corrêa da Silva, R. and Krautz, H.J., 2014. "Emission performance of type-1 pulverized coal flames operating under oxy-fired conditions". Vol. 64, No. 1, pp. 430–440. ISSN 1359-4311. doi:10.1016/j.applthermaleng.2013.12.065.

H. Ferziger, J. and Peric, M., 2002. *Computational Methods for Fluid Dynamics*, Vol. 3. Springer Berlin Heidelberg. ISBN 978-3-540-42074-3. doi:10.1007/978-3-642-56026-2.

Haller, G., 2005. "An objective definition of a vortex". *Journal of Fluid Mechanics*, Vol. 525, pp. 1–26. ISSN 1469-7645, 0022-1120. doi:10.1017/S0022112004002526.

HOLEWA, J., KRÓL, A. and KUKULSKA-ZAJAC, E., 2013. "Biogas as an alternative to natural gas". Vol. 11, No. 67, pp. 1073–1078. ISSN 0009-2886.

Hunt, J.C.R., Wray, A.A. and Moin, P., 1988. "Eddies, streams, and convergence zones in turbulent flows". URL `http://adsabs.harvard.edu/abs/1988stun.proc..193H`.

Leibovich, S., 1978. "The structure of vortex breakdown". Vol. 10, No. 1, pp. 221–246. doi: 10.1146/annurev.fl.10.010178.001253.

Lucca-Negro, O. and O'Doherty, T., 2001. "Vortex breakdown: a review". Vol. 27, No. 4, pp. 431–481. ISSN 0360-1285. doi:10.1016/S0360-1285(00)00022-8.

Mansouri, Z. and Boushaki, T., 2018. "Experimental and numerical investigation of turbulent isothermal and reacting flows in a non-premixed swirl burner". Vol. 72, pp. 200–213. ISSN 0142-727X. doi: 10.1016/j.ijheatfluidflow.2018.06.007.

Merlo, N., Boushaki, T., Chauveau, C., De Persis, S., Pillier, L., Sarh, B. and Gökalp, I., 2013. "Experimental study of oxygen enrichment effects on turbulent non-premixed swirling flames". Vol. 27, No. 10, pp. 6191–6197.

Merlo, N., Boushaki, T., Chauveau, C., Persis, S.D., Pillier, L., Sarh, B. and Gökalp, I., 2014. "Combustion characteristics of methane-oxygen enhanced air turbulent non-premixed swirling flames". Vol. 56, pp. 53–60. ISSN 0894-1777. doi: 10.1016/j.expthermflusci.2013.11.019.

MMA, 2015. "Fundamentos para iNDC brasileira". URL `https://bit.ly/2U3qtl1`.

Penttinen, O., Yasari, E. and Nilsson, H., 2011. "A pimplefoam tutorial for channel flow, with respect to different LES models".

Smagorinsky, J., 1963. "General circulation experiments with the primitive equations". Vol. 91, No. 3, pp. 99–164. ISSN 0027-0644. doi:10.1175/1520-0493(1963)091<0099:GCEWTP>2.3.CO;2.

Sullivan, P.P., McWilliams, J.C. and Moeng, C.H., 1994. "A subgrid-scale model for large-eddy simulation of planetary

boundary-layer flows". Vol. 71, No. 3, pp. 247–276. ISSN 0006-8314, 1573-1472. doi:10.1007/BF00713741.

UNFCCC, 2015. "The Paris Agreement - main page". URL http://unfccc.int/paris$_agreement/items/9485.php$.

Vashahi, F. and Lee, J., 2018. "On the emerging flow from a dual-axial counter-rotating swirler; LES simulation and spectral transition". Vol. 129, pp. 646 – 656. ISSN 1359-4311. doi:https://doi.org/10.1016/j.applthermaleng.2017.10.058.

7. RESPONSIBILITY NOTICE

The authors are the only responsible for the printed material included in this paper.